3-D Time-Domain SAR Imaging of a Forest Using Airborne Multibaseline Data at L- and P-Bands

Othmar Frey, *Member, IEEE*, and Erich Meier, *Associate Member, IEEE*

***Abstract*—In this paper, a time-domain back-projection based tomographic processing approach to a 3-D reconstruction grid is detailed, with the focusing in the third dimension being either modified versions of multilook standard beamforming, robust Capon beamforming, or multiple signal classification. The novel feature of the proposed approach compared to previous synthetic aperture radar (SAR) tomography approaches is that it allows for an approximation-free height-dependent calculation of the sample covariance matrix by exploiting the azimuth-focused data on the 3-D reconstruction grid. The method is applied to experimental multibaseline quad-pol SAR data at L- and P-bands acquired by German Aerospace Center's (DLR) E-SAR sensor: Tomographic images of a partially forested area, including a 3-D voxel plot that visualizes the very high level of detail of the tomographic image, are shown, and an analysis of the focusing performance is given for the full as well as reduced synthetic aperture in the normal direction.**

***Index Terms*—Airborne radar, beamforming, Capon beamformer, forestry, interferometry, L-band, multibaseline, multiple signal classification (MUSIC), P-band, polarimetry, SAR processing, SAR tomography, synthetic aperture radar (SAR), three-dimensional (3-D) imaging, time-domain back-projection (TDBP), tomography.**

I. Introduction

TOMOGRAPHIC imaging using multibaseline (MB) synthetic aperture radar (SAR) data extends the 2-D imaging capabilities of conventional SAR to the third dimension by forming a synthetic aperture (SA) in two dimensions with the result that different scatterers—with whatever scattering mechanisms—that lie within the same range distance in conventional SAR images are no longer inseparable. This property can be exploited for the reconstruction of volumetric structures that are semitransparent to microwaves such as forested areas, as well as for a more detailed imaging of built-up areas and mountainous regions exhibiting layover regions.

Manuscript received June 17, 2010; accepted March 5, 2011. Date of publication April 28, 2011; date of current version September 28, 2011. This work was conducted at the Remote Sensing Laboratories, University of Zurich, Zurich, Switzerland, supported by the Procurement and Technology Center (armasuisse) of the Swiss Federal Department of Defense.

O. Frey was with the Remote Sensing Laboratories, University of Zurich, 8057 Zurich, Switzerland. He is now with the Chair of Earth Observation and Remote Sensing, Institute of Environmental Engineering, Swiss Federal Institute of Technology (ETH) Zurich, 8093 Zurich, Switzerland, and also with GAMMA Remote Sensing AG, 3073 Gümligen, Switzerland (e-mail: otfrey@ethz.ch).

E. Meier is with the Remote Sensing Laboratories, University of Zurich, 8057 Zurich, Switzerland (e-mail: erich.meier@geo.uzh.ch).

Digital Object Identifier 10.1109/TGRS.2011.2128875

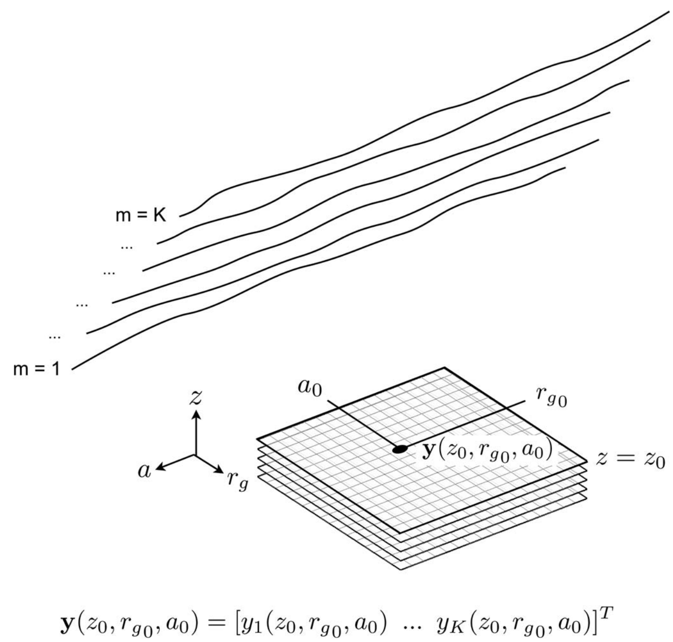

Fig. 1. Tomographic acquisition scenario and the 3-D reconstruction grid. $\mathbf{y}(z_0, r_{g0}, a_0)$ is a vector containing the azimuth-focused signals from K flight tracks at position (z_0, r_{g0}, a_0) of the reconstruction grid. r_g is the ground range, a is the azimuth direction, and z indicates the height within the imaged volume.

It has been shown already in [1] that time-domain-based beamforming in the normal direction is less susceptible to irregular sampling, as found in MB airborne SAR, than fast-Fourier-transform-based methods [2]. Recently, a number of approaches in order to improve the quality of tomographic SAR imaging have been proposed, e.g., [3]–[9]. Beamforming techniques such as the Capon beamformer [10] and multiple signal classification (MUSIC) [11] resolve targets beyond the Fourier resolution. The MUSIC algorithm possesses an inherent robustness against steering vector errors [12]. In the case of the Capon beamformer, an improved resolution and a better sidelobe suppression are obtained if the unknown true steering vector $\mathbf{a}$ is estimated along with the power, a method termed robust Capon beamforming (RCB) [13]. The motivation to process the data entirely in the time domain is driven by the need to achieve maximal focusing quality for both L- and P-band MB data sets. Our time-domain back-projection (TDBP)-based implementation has proven to yield excellent imaging results even in the case of atypical acquisition geometries [14]. In [15], first tomographic images at P-band obtained

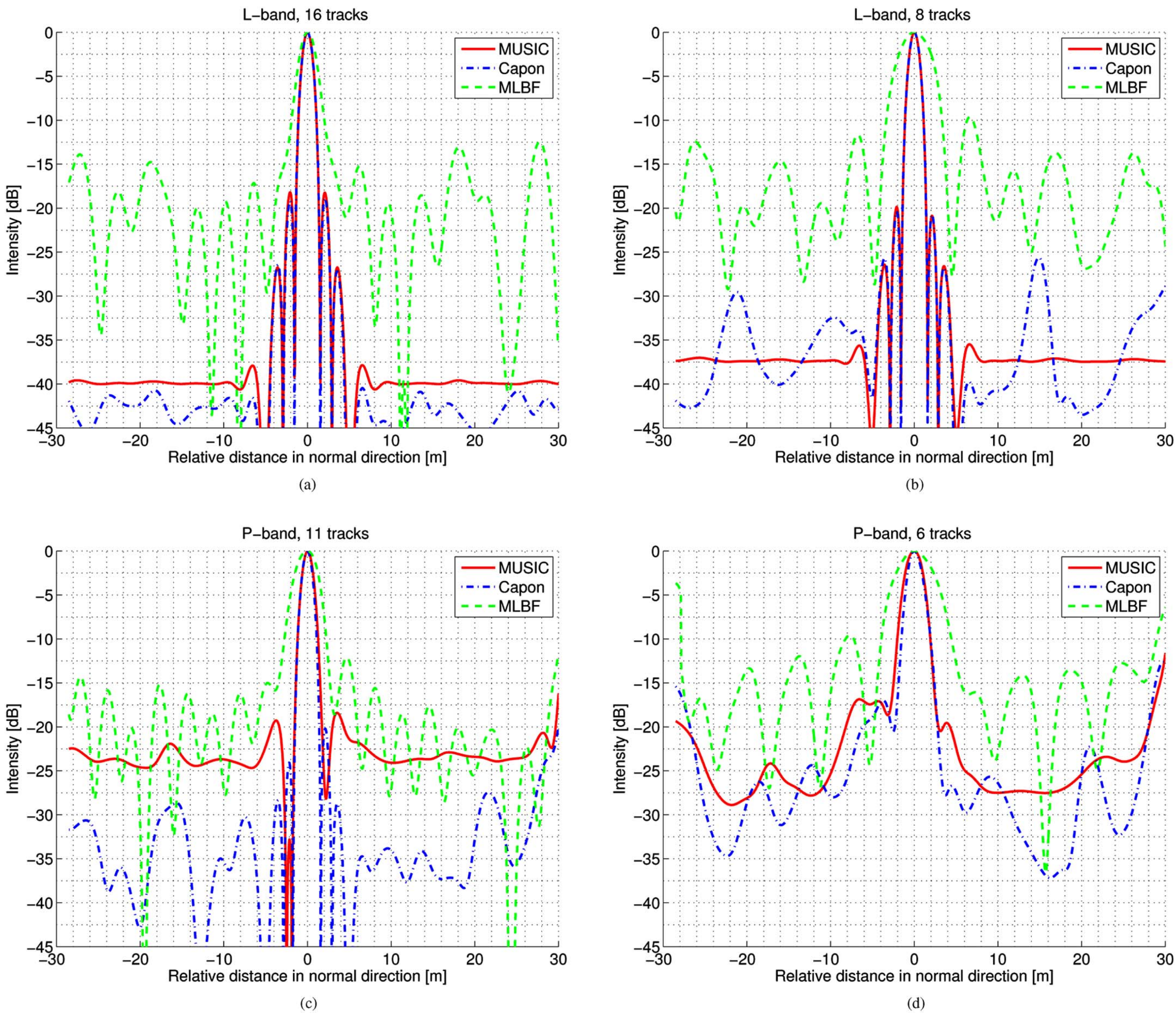

Fig. 2. Impulse responses from a trihedral reflector using three approaches to focus the MB data (HH) in the normal direction: MLBF, RCB, and MUSIC beamforming. (a) L-band, full SA (16 tracks). (b) L-band, reduced SA (eight tracks). (c) P-band, full SA (11 tracks). (d) P-band, reduced SA (six tracks). Twenty looks.

from an airborne MB data set have been presented using the TDBP method to produce 3-D single-look tomograms of a forested area. Despite having achieved a good focusing performance in terms of resolution, the suppression of anomalous sidelobes and ambiguous targets was unsatisfactory.

In this paper, the TDBP-based tomographic processing approach proposed in [15] is extended for multilook beamforming (MLBF), RCB, and MUSIC such that the sample covariance matrices are calculated as a function of height. Given the 3-D reconstruction grid, *truly vertical* tomographic profiles are obtained of a partially forested area. Two airborne MB data sets, at L- and P-bands (see companion paper [16]), are used as experimental data to examine the performance of the different algorithms. While the paper at hand focuses on signal processing aspects of SAR tomography, a thorough analysis of the resulting 3-D data products with respect to the location and type of backscattering sources within a forested area is found in a companion paper [16].

II. Data Model and Focusing Methods

In Fig. 1, a MB flight pattern is depicted representing a typical airborne case where motion deviations from ideally linear and parallel flight tracks are present. In addition, the 3-D reconstruction grid to which the data are focused within the pursued TDBP processing scheme is depicted. There are K individual flight tracks flown in an, ideally, parallel fashion. The vector $\mathbf{y}(z_0, r_{g_0}, a_0)$ contains the demodulated azimuth-focused signals from K flight tracks at position (z_0, r_{g_0}, a_0) of the reconstruction grid. In general, the signal vector $\mathbf{y}$ is

$$\mathbf{y}(z, r_g, a) = [y_1(z, r_g, a) \dots y_K(z, r_g, a)]^T \qquad (1)$$

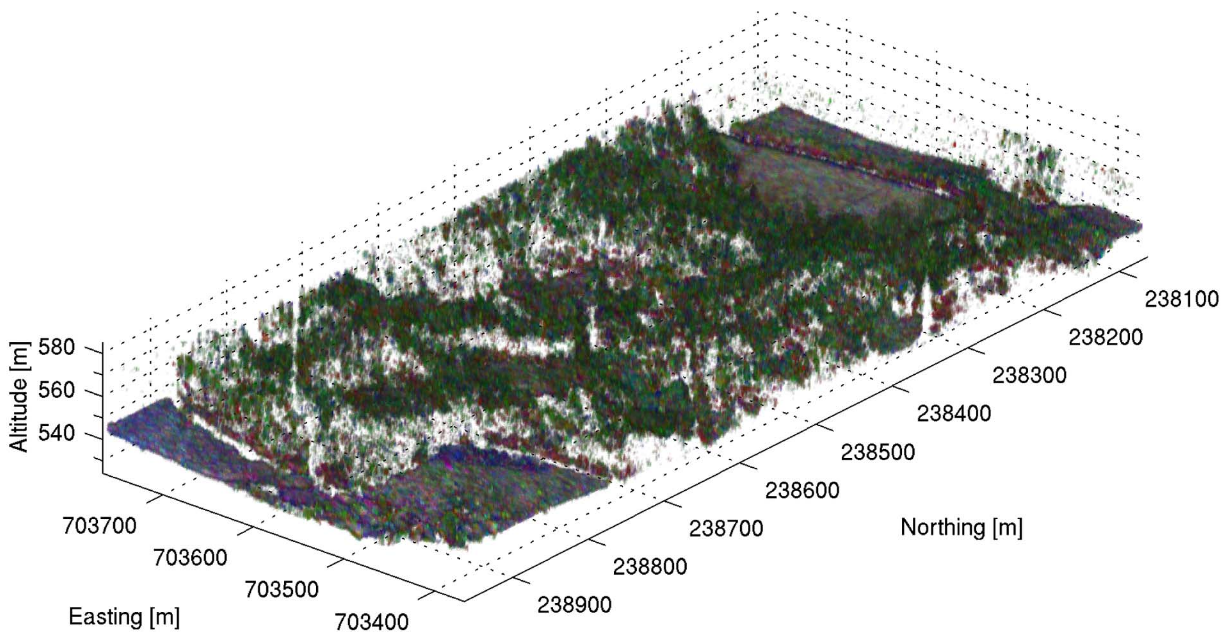

Fig. 3. Tomographic image (3-D voxel plot) of a partially forested area obtained from TDBP-based height-dependent MUSIC beamforming of polarimetric airborne repeat-pass MB SAR data at L-band. Individual scaling. Red (HH), green (HV), and blue (VV). Low intensity = high transparency of the voxel.

where r_g is the ground range position, a is the azimuth position, and z indicates the height within the imaged volume. This representation of the signal vector is given with respect to the coordinate system of the 3-D reconstruction grid. For the sake of readability, the horizontal positioning (r_g and a) of the data vector is omitted in the following. Hence, $\mathbf{y}(z)$ is the signal for a specific voxel at height z. For p sources, the signal vector $\mathbf{y}$, which represents the signal impinging on the across-track positions (repeat-pass flight tracks) of the antenna array synthesized in the normal direction, becomes

$$\mathbf{y} = [\mathbf{a}_1 \quad \dots \quad \mathbf{a}_p] \begin{bmatrix} s_1 \\ \vdots \\ s_p \end{bmatrix} + \mathbf{e} = \mathbf{A}\mathbf{s} + \mathbf{e} \tag{2}$$

where $\mathbf{y}$ is the complex demodulated signal vector, $\mathbf{a}_j = [1\, e^{i\varphi_2} \dots e^{i\varphi_K}]^T$ are called the steering vectors, with $\varphi_m = -2k_c(r_m - r_1)$, $m = 1 \dots K$ (k_c is the central wavenumber and r_m is the range distance from the backscattering element to the mth sensor position), and $\mathbf{e} = [e_1 \dots e_K]^T$ denotes uncorrelated noise. $s = \alpha e^{i\phi}$ is the signal by a particular source (backscattering element). $\mathbf{y}$ and $\mathbf{e}$ are assumed to be zero-mean complex Gaussian distributed with covariance matrices $\mathbf{R} = \mathbf{y}\mathbf{y}^H$ and $\sigma^2\mathbf{I}$, respectively; $(.)^H$ stands for the complex conjugate transpose of a matrix, and $\mathbf{I}$ is the identity matrix.

MLBF has been applied using the time-domain back-projection based approach sketched in [17]. The main steps to compute the location of the scatterers based on MUSIC [11] are the following: 1) determine the eigen decomposition $\mathbf{R} = \mathbf{U}\mathbf{D}\mathbf{U}^H$; 2) permute matrix elements such that the eigenvalues in $\mathbf{D}$ are sorted in nonincreasing order $\gamma_1 \geq \gamma_2 \geq \dots \geq \gamma_K$, with the matrix of eigenvectors $\mathbf{U}$ adjusted accordingly; 3) set a relative threshold [8] for the eigenvalue that separates signal and noise subspaces; and 4) estimate the locations of the sources by

$$\hat{P}_M = \frac{1}{\mathbf{a}^H \mathbf{G}\mathbf{G}^H \mathbf{a}} \tag{3}$$

with $G = [\mathbf{u}_{p+1} \dots \mathbf{u}_K]$ containing the noise space eigenvectors. Li *et al.* [18] and Stoica *et al.* [13] have proposed a robust version of the Capon beamformer, and its application in the context of SAR tomography is reported in [19]. Their approach has been used in this paper for RCB, and in the following, we indicate the steps to compute the robust Capon beamformer, which is found by solving the following expression [18]: $\max_{\mathbf{a},P_C} P_C$ subject to $\mathbf{R} - P_C\mathbf{a}\mathbf{a}^H, (\mathbf{a} - \bar{\mathbf{a}})^H \mathbf{C}^{-1}(\mathbf{a} - \bar{\mathbf{a}}) \leq 1$. Using (1) the fact that $P_C = 1/(\mathbf{a}^H\mathbf{R}^{-1}\mathbf{a})$ maximizing P_C is equivalent to minimizing $\mathbf{a}^H\mathbf{R}^{-1}\mathbf{a}$, (2) assuming that $\mathbf{a} = 0$ is not part of the uncertainty ellipsoid, i.e., the solution to $\mathbf{a}$ will lie on the boundary of the ellipsoid, and, furthermore, (3) as there is no sufficient *a priori* information about the variance of the individual components of the steering vector, the covariance matrix $\mathbf{C}$ is set to $\mathbf{C} = \epsilon\mathbf{I}$, and the estimation problem reduces to the following quadratic problem with a quadratic equality constraint $\min_{\mathbf{a}} \mathbf{a}^H\mathbf{R}^{-1}\mathbf{a}$ subject to $\|\mathbf{a} - \bar{\mathbf{a}}\|^2 = \epsilon$. This expression can then be solved efficiently by using the Lagrange multiplier approach $F(\mathbf{a}, \lambda) = \mathbf{a}^H\mathbf{R}^{-1}\mathbf{a} + \lambda \cdot (\|\mathbf{a} - \bar{\mathbf{a}}\|^2 - \epsilon)$. The robust Capon beamformer is computed as follows:

1) Eigen decomposition of $\mathbf{R} = \mathbf{U}\mathbf{D}\mathbf{U}^H$ and $\mathbf{b} = \mathbf{U}^H\bar{\mathbf{a}}$.
2) Solve $\sum_{m=1}^{K}(|b_m|^2/(1 + \lambda\gamma_m)^2) = \epsilon$ for the Lagrange multiplier λ, given the fact that there is a unique solution in the interval $[\lambda_{low}, \lambda_{up}]$ (see [20]), where $\lambda_{low} = (\|\bar{\mathbf{a}}\| - \sqrt{\epsilon})/(\gamma_1\sqrt{\epsilon})$ and $\lambda_{up} = (\|\bar{\mathbf{a}}\| - \sqrt{\epsilon})/(\gamma_K\sqrt{\epsilon})$.
3) Estimate ($\hat{\mathbf{a}}$) the unknown steering vector $\mathbf{a}$: $\hat{\mathbf{a}} = \bar{\mathbf{a}} - \mathbf{U}(\mathbf{I} + \lambda\mathbf{D})^{-1}\mathbf{b}$.

4) Using the knowledge that the true steering vector $\mathbf{a}$ satisfies the condition $\mathbf{a}^H\mathbf{a} = K$, the estimated power finally yields [20]

$$\hat{P}_C = \frac{\hat{\mathbf{a}}^H\hat{\mathbf{a}}}{K\hat{\mathbf{a}}^H\mathbf{U}\mathbf{\Gamma}^{-1}\mathbf{U}^H\hat{\mathbf{a}}}. \tag{4}$$

III. Results

The basis for a comparison of the focusing quality in the normal direction is given by means of an analysis of the different impulse responses obtained by varying the following parameters: 1) focusing technique (MLBF, RCB, and MUSIC beamforming); 2) full and reduced (half) lengths of the SA in the normal direction; and 3) frequency (L-band and P-band MB data). The respective impulse responses as a function of the relative distance in the normal direction are shown in Fig. 2. The impulse responses have been measured based on a trihedral reflector.

Fig. 3 depicts a 3-D voxel plot representation of the partially forested area under study obtained from TDBP-based height-dependent MUSIC beamforming of the polarimetric MB SAR data at the L-band. Fig. 4 contains vertical slices through the volume for the RCB- and MUSIC-focused tomograms at the L- and P-bands. In addition, the tomographic slices are overlaid by a digital elevation model (DEM) and a digital surface model (DSM) created from airborne laser scanning data (TopoSys GmbH).

IV. Discussion and Conclusion

1) Analysis of the Impulse Response: Compared to MLBF, both techniques, RCB and MUSIC beamforming, deliver a much improved suppression of the sidelobes in all cases, the full and the reduced SA as well as at both frequencies. Furthermore, RCB and MUSIC are able to maintain a high resolution also for the reduced SA, whereas for MLBF, the resolution degrades considerably. Using RCB or MUSIC, the sidelobes are low (this is also visible in the vertical profile plot when examining the nonforested areas). The remaining calibration errors in the steering vectors can be mitigated by using RCB or MUSIC, which are both robust against miscalibration, and they therefore leave the focusing quality unaffected.

2) Tomographic Images: A tomographic 3-D voxel image of a forested area at a very high level of detail is obtained. For instance, gaps in the canopy due to features like small forest roads of a width of a few meters only are clearly visible at the given ground range azimuth resolution. Other techniques that have been proposed in the literature to characterize forest by either SAR tomography or polarimetric SAR interferometry approaches work with an averaging at a completely different scale (Tebaldini [9], for instance, used a 50 m $\times$ 50 m averaging window, corresponding to about 350 independent looks, whereas 20 looks have been applied in this paper). It can be stated that, at the L-band, both the canopy layer and the ground level are detected. Also, at the P-band, the canopy and the ground beneath are well separated. However, backscattering from the crown layer occurs only sparsely compared to the L-band data. On the other hand, the ground level is virtually continuously detected at the P-band, indicating a high level of foliage penetration.

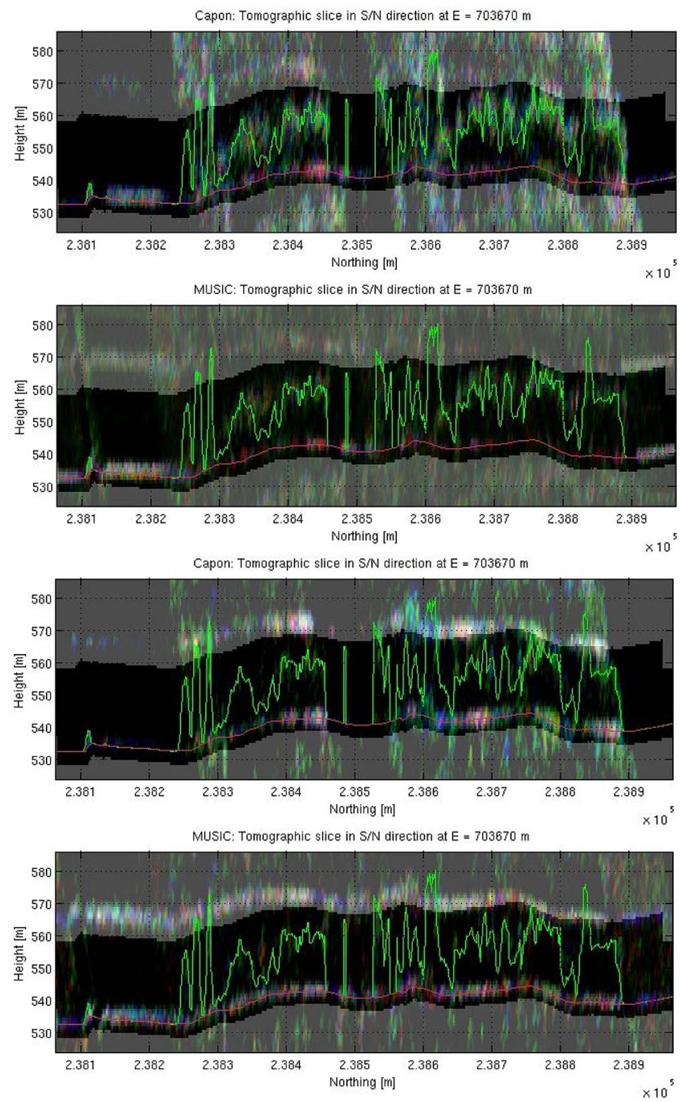

Fig. 4. Vertical slices through a 3-D volume of a forested area obtained from quad-pol MB at L- and P-bands. Red (HH), green (HV), and blue (VV). Individual scaling. (Grayed area) Ambiguous target regions. The tomographic slices run in south-northern direction and are overlaid by the DEM/DSM (solid red/green line) from ALS. Top down: RCB and MUSIC at L- and P-bands, respectively.

Concluding, a time-domain-based tomographic SAR imaging method has been presented that encompasses MLBF, RCB, and MUSIC beamforming. An example of a MUSIC-focused L-band MB data set, given as a 3-D voxel plot, demonstrates the very high level of detail that is achieved compared to other methods described in the literature so far. In our example, features such as gaps in the canopy can be observed at locations where the forest is intersected by narrow roads. With the help of an exemplary vertical profile provided at L- and P-bands, a qualitative impression of the high level of detail is obtained, whereas good focusing performance is illustrated by means of a quantitative analysis of the impulse responses obtained from the different processing methods and configurations. For a localization of the main scattering sources, e.g., for ground detection at the P-band, either RCB or MUSIC can be applied even with a reduced SA in the normal direction. For the first time, high-resolution tomographic SAR images of the same forested area were presented at both the L-band and P-band.

Acknowledgment

The authors would like to thank the E-SAR/F-SAR team at the German Aerospace Center (DLR) for their cooperation and technical support. They would also like to thank P. Wellig at armasuisse for his wide support and cooperation.

References

[1] M. Nannini and R. Scheiber, "A time domain beamforming algorithm for SAR tomography," in *Proc. 6th EUSAR*, 2006, pp. 1–4.
[2] A. Reigber and A. Moreira, "First demonstration of airborne SAR tomography using multibaseline L-band data," *IEEE Trans. Geosci. Remote Sens.*, vol. 38, no. 5, pp. 2142–2152, Sep. 2000.
[3] F. Lombardini and A. Reigber, "Adaptive spectral estimation for multibaseline SAR tomography with airborne L-band data," in *Proc. IEEE Int. Geosci. Remote Sens. Symp.*, 2003, vol. 3, pp. 2014–2016.
[4] G. Fornaro, F. Serafino, and F. Soldovieri, "Three-dimensional focusing with multipass SAR data," *IEEE Trans. Geosci. Remote Sens.*, vol. 41, no. 3, pp. 507–517, Mar. 2003.
[5] M. Nannini and R. Scheiber, "Height dependent motion compensation and coregistration for airborne SAR tomography," in *Proc. IEEE Int. Geosci. Remote Sens. Symp.*, Jul. 2007, pp. 5041–5044.
[6] F. Lombardini and M. Pardini, "3-D SAR tomography: The multibaseline sector interpolation approach," *IEEE Geosci. Remote Sens. Lett.*, vol. 5, no. 4, pp. 630–634, Oct. 2008.
[7] G. Fornaro and A. Pauciullo, "LMMSE 3-D SAR focusing," *IEEE Trans. Geosci. Remote Sens.*, vol. 47, no. 1, pp. 214–223, Jan. 2009.
[8] M. Nannini, R. Scheiber, and A. Moreira, "Estimation of the minimum number of tracks for SAR tomography," *IEEE Trans. Geosci. Remote Sens.*, vol. 47, no. 2, pp. 531–543, Feb. 2009.
[9] S. Tebaldini, "Algebraic synthesis of forest scenarios from multibaseline PolInSAR data," *IEEE Trans. Geosci. Remote Sens.*, vol. 47, no. 12, pp. 4132–4142, Dec. 2009.
[10] J. Capon, "High-resolution frequency-wavenumber spectrum analysis," *Proc. IEEE*, vol. 57, no. 8, pp. 1408–1418, Aug. 1969.
[11] R. O. Schmidt, "Multiple emitter location and signal parameter estimation," *IEEE Trans. Antennas Propag.*, vol. AP-34, no. 3, pp. 276–280, Mar. 1986.
[12] P. Stoica, Z. Wang, and J. Li, "Extended derivations of MUSIC in the presence of steering vector errors," *IEEE Trans. Signal Process.*, vol. 53, no. 3, pp. 1209–1211, Mar. 2005.
[13] P. Stoica, Z. Wang, and J. Li, "Robust Capon beamforming," *IEEE Signal Process. Lett.*, vol. 10, no. 6, pp. 172–175, Jun. 2003.
[14] O. Frey, C. Magnard, M. Rüegg, and E. Meier, "Focusing of airborne synthetic aperture radar data from highly nonlinear flight tracks," *IEEE Trans. Geosci. Remote Sens.*, vol. 47, no. 6, pp. 1844–1858, Jun. 2009.
[15] O. Frey, F. Morsdorf, and E. Meier, "Tomographic imaging of a forested area by airborne multi-baseline P-band SAR," *Sensors*, vol. 8, no. 9, pp. 5884–5896, Sep. 2008.
[16] O. Frey and E. Meier, "Analyzing tomographic SAR data of a forest with respect to frequency, polarization, and focusing technique," *IEEE Trans. Geosci. Remote Sens.*, vol. 49, no. 10, pp. 3648–3659, Oct. 2011.
[17] O. Frey and E. Meier, "Combining time-domain back-projection and Capon beamforming for tomographic SAR processing," in *Proc. IEEE Int. Geosci. Remote Sens. Symp.*, 2008, pp. 445–448.
[18] J. Li, P. Stoica, and Z. Wang, "On robust Capon beamforming and diagonal loading," *IEEE Trans. Signal Process.*, vol. 51, no. 7, pp. 1702–1715, Jul. 2003.
[19] A. Jakobsson, F. Gini, and F. Lombardini, "Robust estimation of radar reflectivities in multibaseline InSAR," *IEEE Trans. Aerosp. Electron. Syst.*, vol. 41, no. 2, pp. 751–758, Apr. 2005.
[20] P. Stoica and R. L. Moses, *Spectral Analysis of Signals*. Upper Saddle River, NJ: Prentice-Hall, 2005.

Othmar Frey (S'04–M'08) received the M.Sc. degree in geomatic engineering from Swiss Federal Institute of Technology (ETH) Zurich, Zurich, Switzerland, in 2002 and the Ph.D. (Dr. sc. nat.) degree (with distinction) in remote sensing from the University of Zurich, Zurich, in 2010.

From 2002 to 2010, he was a Research Associate with the Remote Sensing Laboratories, University of Zurich, where he worked on a geometric error budget analysis for TerraSAR-X data products and on atmospheric effects in synthetic aperture radar (SAR) data until 2003/2004. Since then, he has mainly been working in the field of SAR signal processing with emphasis on airborne SAR imaging and SAR tomography. He has developed and implemented SAR signal-processing software that allows for end-to-end data processing of advanced imaging modes, such as airborne multibaseline SAR and SAR data acquisitions from nonlinear flight tracks. Since 2011, he has been with the Chair of Earth Observation and Remote Sensing, Institute of Environmental Engineering, ETH Zurich, as a Senior Research Scientist, and with GAMMA Remote Sensing AG, Gümligen, Switzerland.

Dr. Frey has contributed to invited sessions on SAR tomography at the 2008 European Conference on Synthetic Aperture Radar (EUSAR) and the IEEE International Geoscience and Remote Sensing Symposia in 2008, 2009, and 2010. He was the recipient of the 3rd Place Student Paper Award at the 2010 EUSAR Conference in Aachen, Germany, and the ETH medal for an outstanding M.Sc. thesis. He was the corecipient of the Best Paper Award at the ISPRS Workshop Laserscanning and Silvilaser 2007 in Helsinki, Finland.

Erich Meier (A'09) received the M.Sc. degree in geography and the Ph.D. (Hons.) degree in remote sensing from the University of Zurich, Zurich, Switzerland, in 1982 and 1989, respectively.

From 1979 to 1982, he was a Research Assistant with the Remote Sensing Section and, from 1982 to 1983, with the GIS Laboratory, Department of Geography, University of Zurich. From 1983 to 2006, he was a Research Scientist with the Remote Sensing Laboratories (RSL), Department of Geography, University of Zurich, where he is currently the Research Section Head involved in teaching as well as in research in digital image processing, software development for computer graphics, and radiometric and geometric calibrations of SAR and optical imagery. Since 2000, he has been the Head of the SARlab, a research group within RSL. The main research interests of this group are the development of new focusing algorithms for SAR data from UHF to millimeter wave, interferometry, polarimetry, and moving target indication algorithms, as well as calibration and validation activities for spaceborne and airborne systems. He is responsible for the research strategies as well as the organization of the team. He is a Consultant on behalf of several national and international organizations and private companies.